Journal of Marine Systems 240 (2023) 103891

Contents lists available at ScienceDirect

Journal of Marine Systems

journal homepage: www.elsevier.com/locate/jmarsys

Spring phytoplankton distributions and primary productivity in waters off northern Norway

R. Meng [a], W.O. Smith Jr [a,b,*], S.L. Basedow [c]

[a] School of Oceanography, Shanghai Jiao Tong University, Shanghai, China
[b] Virginia Institute of Marine Science, William & Mary, Gloucester Pt., VA, USA
[c] University in Tromsø, The Arctic University of Norway, Tromsø, Norway

ARTICLE INFO

Keywords:
Phytoplankton
Primary productivity
Calanus finmarchicus
Chlorophyll
Norway

ABSTRACT

The distributions of phytoplankton, zooplankton and hydrographic features off the coast of northern Norway were assessed in late April – early May 2019 using ship-based observations (CTD casts and Moving Vessel Profilers) and autonomous vehicles. A satellite chlorophyll climatology was generated to place our in-situ observations within a longer temporal sequence. Substantial spatial and temporal variability on all scales was observed in both the observations and climatology. Spring phytoplankton accumulation usually is initiated in the south on the continental shelf, and advanced in a northerly direction through time. Accumulations in the surface layer of deeper waters off the continental shelf occurred 2–3 weeks later than those on the shelf. During our survey, primary productivity was greatest in offshore waters where nutrients were not depleted and exceeded 2 g C m^{-2} d^{-1}. The greatest *Calanus finmarchicus* abundances were associated with low chlorophyll concentrations, suggesting a major impact of grazing on phytoplankton biomass, but estimates of phytoplankton growth and zooplankton removal suggested that *Calanus* was responsible for a variable fraction (3–69%) of the daily chlorophyll changes. Vertical changes in chlorophyll were related to physical features during some transects, but to grazing and sinking in others. Understanding the spatial and temporal variations of the coupling of phytoplankton to zooplankton is essential to effective management of this important commercial species in Norwegian waters.

1. Introduction

Waters off the Norwegian coast have received considerable attention due to the large populations of commercially valuable species [e.g., Northeast Arctic cod (*Gardus morhua*), the copepod *Calanus finmarchicus*, and Norwegian herring (*Clupea harengus*)] that have supported local and regional fisheries for centuries. Understanding the distribution of these species, and the food web that supports them, is critical to an effective management strategy. Phytoplankton distributions in the region have also been studied, given that phytoplankton support the food web in which *C. finmarchicus* appears to serve as the dominant grazer and food for higher trophic species (as well as being commercially harvested). In general, coastal waters support a spring bloom that reaches its maximum in late April, while chlorophyll concentrations in offshore waters become maximal about one month later (Bagøien et al., 2012). Substantial spatial and temporal variations occur among years, as winds, fresh-water inputs from fjords, storms, and bathymetry all influence local growth and distributions of phytoplankton.

Phytoplankton biomass is often assessed by measuring chlorophyll concentrations. Methods to measure chlorophyll *a*re well standardized; furthermore, as fluorescence is also a routine parameter on a variety of platforms, those values can be calibrated against discrete chlorophyll measurements and converted into chlorophyll concentrations. Examples of platforms which routinely measure fluorescence on small vertical and horizontal scales are CTDs, autonomous vehicles (such as gliders and wave gliders) and moving vessel profilers. The different sampling technologies allow for a greater spatial and temporal resolution of phytoplankton biomass and provide new insights into the processes controlling phytoplankton growth and accumulation (Mahadevan et al., 2012; Kaufman et al., 2014; Ryan-Keogh and Smith Jr., 2021).

Primary productivity of phytoplankton during photosynthesis has traditionally been measured using radiotracer techniques (e.g., Steemann Nielsen, 1952; Marra, 2009; Marra et al., 2021), in which samples are collected from known isolumes, ^{14}C-bicarbonate added, and

* Corresponding author at: School of Oceanography, Shanghai Jiao Tong University, Shanghai, China
E-mail addresses: mengrui0101@sjtu.edu.cn (R. Meng), wos@vims.edu (W.O. Smith), sunnje.basedow@uit.no (S.L. Basedow).

https://doi.org/10.1016/j.jmarsys.2023.103891
Received 7 November 2022; Received in revised form 29 March 2023; Accepted 10 April 2023
Available online 13 April 2023

incorporation quantified after samples are incubated in a defined irradiance on the deck of a ship. These measurements are an important system variable, in that they describe the rate of growth of phytoplankton and put an upper limit on energy available within the food web. However, considerable limitations and uncertainties remain in assessing and comparing isotopic measurements. For example, collecting seawater and placing the samples in bottles removes phytoplankton from their natural, turbulent environment and can induce serious bottle effects due to the death of microzooplankton grazers (Eppley, 1982). The size of bottles also precludes the inclusion of macro-zooplanktonic grazers such as copepods, thus altering rates of nutrient cycling. The time of the incubation start also influences net fixation, as does the length of incubation (Marra, 2009), and vertical temperature variations and their impacts on photosynthesis are usually not considered or controlled (Ma and Smith Jr., 2022). As a result, it is difficult to unambiguously assign the measured isotopic rate as being a measure of net or gross photosynthesis; such measurements clearly cannot be completed on the same space and time scales that are sampled by platforms measuring fluorescence, oxygen, temperature and salinity.

An alternative method has been introduced that uses oceanographic data to estimate primary productivity: a vertically-resolved productivity model (Behrenfeld and Falkowski, 1997a, 1997b; Friedrichs et al., 2009; Lee et al., 2015). This procedure has been applied to satellite data, as the model inputs required are sea surface temperature, irradiance, and surface chlorophyll concentrations, all parameters that can be measured remotely. The model can also be applied within the water column to estimate vertically resolved productivity using the same parameters along with an assumed photosynthetic response (Ma and Smith Jr., 2022). As these variables are routinely collected using CTDs, gliders and profilers, estimates of primary production on small vertical and horizontal scales can be made during surveys of specific areas and provide insights into the variability of productivity on the same scales as biomass. While there are similarities between the models, both have limitations and assumptions; however, they provide estimates of the rates of carbon fixation in a specific area of the ocean.

In April–May 2019 we conducted a cruise off the Lofoten coast to assess the distribution of phytoplankton, the physical processes occurring on the continental shelf, shelf-break and slope, and their impacts on the copepod *Calanus finmarchicus*. *C. finmarchicus* is a critically important species in the region, as it is the keystone species of the regional food web and commercially harvested as a result of the massive aggregations that occur (Basedow et al., 2019). These aggregations can be observed from space due to the animal's pigments, further emphasizing the importance of this species to the region (Basedow et al., 2019; Dong et al., 2021). Understanding the relationship of both physical factors and phytoplankton distributions to copepod growth and development is important to managing this resource. Given its substantial abundance, we hypothesized that *Calanus* grazing would be an important phytoplankton loss process. The objective of our survey was to investigate how physical, biogeochemical and biological processes are coupled on the Norwegian shelf-slope system. We also placed our results within a regional climatology to determine the stage of bloom development in the shelf-slope area. Primary productivity was estimated by two different models to constrain the turnover of phytoplankton and to provide a means to estimate the impact of grazing by zooplankton. We focused on the relationships among hydrography, phytoplankton and zooplankton distributions and their variability in space and time.

2. Materials and methods

2.1. Study region

The study site was the continental shelf and shelf slope area between 67.7 and 69.7°N and 9.5 to 15.8°E off northern Norway (Fig. 1). The main currents in this area are the Norwegian Coastal Current (NCC) and Norwegian Atlantic Slope Current (NwASC; Dong et al., 2021). NCC is a buoyancy-driven, northward flowing current trapped near the Norwegian coast. It originates at the Baltic entrance to the Skagerrak and receives coastal freshwater inputs as it flows north (Skagseth et al., 2011). The NwASC carries warm, saline, nutrient-rich water along the

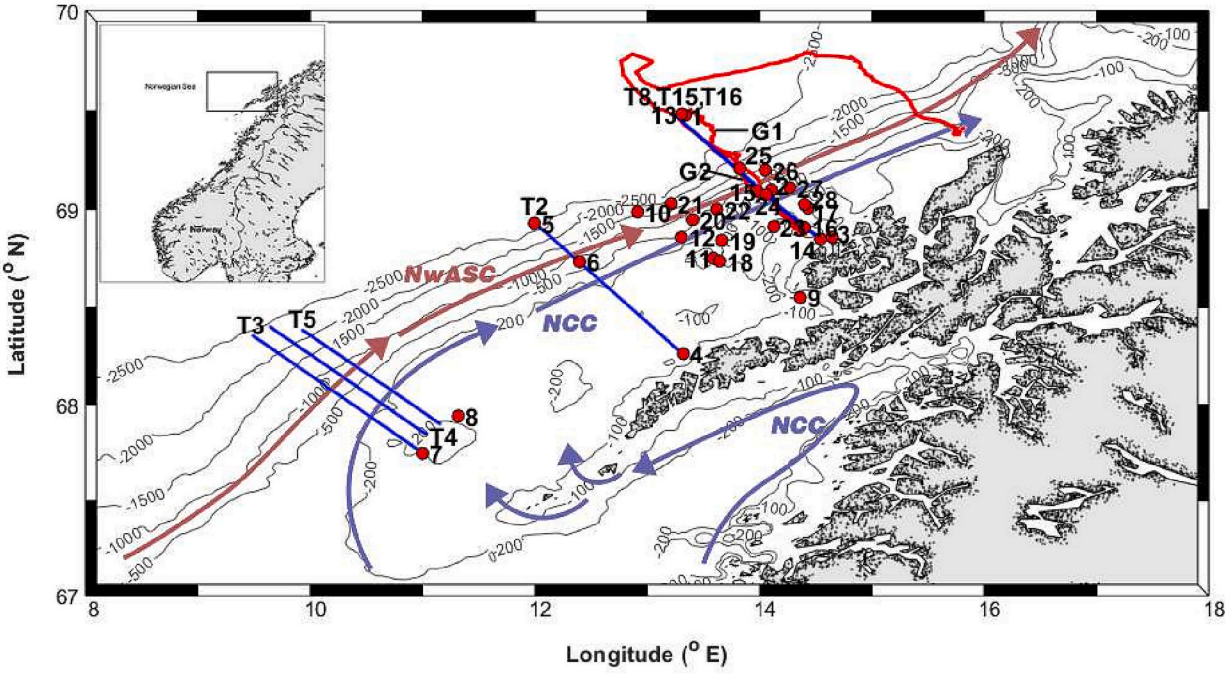

Fig. 1. Location of sampling stations and transects. Map showing the CTD station locations (red dots) and the transects occupied by the moving vessel profiler (blue lines) and the glider (red curves). Approximate location of currents [the Norwegian Coastal Current (NCC) in blue arrows and the Norwegian Atlantic Slope Current (NwASC) in red arrows] are also shown. The inset shows the location of the study off the coast of Norway. (For interpretation of the references to color in this figure legend, the reader is referred to the web version of this article.)

Norwegian continental shelf break. The NCC and NwASC carry cold and fresh Norwegian Coastal Water (NCW, S < 34.5) and warm and more saline North Atlantic Water (NAW, S > 35) along the Norwegian continental shelf, respectively (Mork et al., 1981; Pedersen et al., 2005). A salinity front forms between the two water masses and is usually located near the shelf break, delineated by the 34.8 isohaline (Sætre, 1999).

2.2. Sample collection

Data were collected during spring, 2019 (April 27 – May 12) from the *R.V. Helmer Hanssen* near the Lofoten-Vesterålen Islands as part of the STRESSOR program (Collaborative Studies of Two Resource Ecosystems in Shelf, Slope and Oceanic Regions of the Norwegian and South-China Seas; Fig. 1). Surface photosynthetically active radiation (PAR) was measured continuously using an on-deck Biospherical/Licor 4Π sensor. Water samples were obtained at 28 stations (Fig. 1) using a CTD-rosette system equipped with Niskin bottles and an in situ PAR sensor. A total of 17 Moving Vessel Profiler (MVP; Rolls Royce Canada, Ltd.) transects were completed across continental shelf and slope; seven were used in this analysis. Finally, a glider (Seaglider, Kongsberg) equipped with a WetLabs ECO puck to collect fluorescence and optical backscatter data sampled in transects roughly perpendicular to the shelf (Fig. 1). Dates and locations (start and end) of all analyzed transects are listed in Supplementary Material (Table A1).

2.3. CTD sampling

A SeaBird 911+ CTD was deployed on a rosette from the surface to the bottom at shallow stations, or through 600 m at deeper stations. All sensors were calibrated prior to the cruise. Water samples for nutrients, chlorophyll, particulate organic carbon and nitrogen, and biogenic silica were collected from 5-L Niskin bottles mounted on the rosette frame. Nutrient samples (50 mL) at selected depths (0, 5, 10, 20, 50 m and bottom) were collected in centrifuge tubes (tubes were rinsed with seawater three times before samples were collected), and frozen upright at −20 °C. Nutrient concentrations (nitrate, nitrite, phosphate, silicate) were analyzed using automated techniques at University of Tromsø using a QuAAtro39 Seal autoanalyzer.

Chlorophyll, particulate organic carbon and nitrogen, and biogenic silica were collected in opaque, acid-cleaned bottles. Chlorophyll samples (generally 250 mL) were filtered through Whatman GF/F filters under low vacuum (<½ atm) and the filters immediately frozen for later analyses. In the laboratory samples were extracted in methanol and analyzed fluorometrically on a Turner Designs fluorometer calibrated with commercially purified chlorophyll *a*. Particulate organic carbon/nitrogen samples were filtered through combusted (450 °C for 4 h) 25 mm GF/F filters under low pressure, rinsed with ca. 5 mL 0.01 N HCl in filtered seawater, placed in combusted glass vials, covered with combusted aluminum foil, and dried at 60 °C for later analyses (Gardner et al., 2000). Blanks were filters through which a few mL of seawater had been filtered and processed identically. All samples were analyzed on a Unicube Elementar elemental analyzer using sulfanilamide as a standard. Biogenic silica samples were filtered through 0.6 μm polycarbonate filters (Whatman), folded, placed in glassine envelopes, dried at 60 °C and returned to the laboratory for analyses. Filters were digested in NaF and the resultant silicic acid measured spectrophotometrically (Brzezinski and Nelson, 1989).

CTD fluorescence data were calibrated by correlating discrete sample chlorophyll concentrations collected at known depths with fluorescence values at the same depths ($n = 189$). The resulting significant regression [Chl (mg m^{-3}) = 0.56 × Fl- 0.25; $R^2 = 0.89$] was applied to all fluorescence data, providing a detailed vertical description (1-m resolution) of phytoplankton biomass.

2.4. MVP sampling

High resolution cross-shelf transects were obtained using a moving vessel profiler fitted with a Seabird CTD (sampling rate of 25 Hz), a fluorescence sensor and LOPC (Laser Optical Plankton Counter; sampling rate 2 Hz) to obtain information on hydrological and particle properties. The MVP was towed behind the ship as it steamed 6–7 kts, continuously taking nearly vertical profiles in the upper 600 m before returning to the surface. The MVP transects were between 80 and 90 km long and sampled the shelf, slope, and deep water (Fig. 1). All transects were completed during darkness. MVP fluorescence data were calibrated in a manner similar to those from the CTD casts. Discrete chlorophyll samples ($n = 45$) were collected at the surface from the ship's flowing seawater system (which had been cleaned prior to the cruise) when the MVP reached the surface. The resulting significant regression between chlorophyll *a*nd fluorescence [Chl (mg m^{-3}) = 97.2 × Fl + 12.8; $R^2 = 0.85$] was applied to all MVP data. CTD data were recorded with a high frequency (25 Hz) and were converted to the frequency of the LOPC data (2 Hz).

The LOPC provides high spatial resolution measurements of particle sizes. It measures the numbers and equivalent spherical diameter (ESD) of particles between 100 μm and ca. 3 cm (Herman et al., 2004), and additional features for particles > ca. 800 μm ESD, but does not provide taxonomic or activity data of the particles. Previous investigations in this region have shown there are relatively few zooplankton species; furthermore, the LOPC has been shown to provide reliable *Calanus finmarchicus* copepodite abundance estimates (Basedow et al., 2008; Gaardsted et al., 2010). LOPC ESD data ranging between 1.0 and 2.0 mm were selected as an estimate of *C. finmarchicus* adult and stage V copepodite abundance (Basedow et al., 2013). In addition, an attenuation index (AI) ≥ 0.4 was applied when computing *C. finmarchicus* abundance from MEPs (multi-element particle) data to exclude transparent MEPs such as marine snow (Basedow et al., 2013). Zooplankton concentrations were estimated by normalizing LOPC counts by the volume of filtered water. Data from down-profiles was used for abundance calculation, as upward-profiles tend to yield less precise values for water flow through the LOPC.

2.5. Glider sampling

An autonomous underwater vehicle (glider) was deployed to collect observations of ocean water properties and estimates of velocity fields. The glider oscillated along transects roughly perpendicular to the shelf break (Fig. 1) and profiled from the surface to 1000 m (or close to the bottom). Unfortunately, no CTD casts were taken in proximity to the glider, so the glider fluorescence data could not be reliably converted to chlorophyll units. Therefore, fluorescence data are reported in arbitrary units and used to represent relative phytoplankton concentrations. Only data from the upper 200 m (temperature, salinity, and fluorescence) were used.

2.6. Primary productivity estimates

A bio-optical model to estimate vertically resolved primary productivity was developed using the temperature and chlorophyll distributions obtained from both the CTD and MVP. The model was based on the formulations of Behrenfeld and Falkowski (1997a, 1997b) where vertically-resolved (at 1-m intervals) productivity is a function of temperature, irradiance (PAR), an assumed photosynthetic response, and chlorophyll concentration (Eq. (1)):

$$PP = C_z \times P^B_{opt} \times f(E_0) \quad (1)$$

where PP is integrated primary productivity (mg C m^{-3} d^{-1}), C_z is chlorophyll concentration (mg chl m^{-3}) at depth z (m), P^B_{opt} the maximum photosynthetic rate (mg C (mg chl)$^{-1}$ $h^{-1)}$, and $f(E_0)$ the

photon flux density at each depth (measured directly by the CTD PAR sensor). Not all CTD casts or MVP profiles were completed during the day; therefore, direct measurements of PAR attenuation within the water column were not always available. To generate potential irradiance attenuation profiles, the relationship between chlorophyll *a* and attenuation (Morel, 1974; Morel, 1998) was used and corrected for an offset from casts conducted during the day. We believe this offset was due to dissolved organic carbon that originated from the freshwater inflows (Smith Jr. et al., 2021). A photosynthesis-irradiance response was assumed (Eq. (2)) (Platt and Jassby, 1976):

$$P_z^B = P_{opt}^B \times tanh\left[E_z/E_k\right] \quad (2)$$

E_k values were taken from Bouman et al. (2018), with $E_k = 0.15 \times E_0$, when E_0 (surface PAR) < 100 μmol photons m^{-2} s^{-1}, and $E_k = 0.25 \times E_0$ when $E_0 > 100$ μmol photons m^{-2} s^{-1}. P_{opt}^B was derived using the 7-order regression derived by Behrenfeld and Falkowski (1997b) that was based on 1698 radioisotope profiles measured throughout the ocean. A photoinhibition term based on the same data set was also included that reduced productivity when daily irradiance was >3 mol photons m^{-2} d^{-1} (Behrenfeld and Falkowski, 1997b). E_z (irradiance at depth z) values were derived from the in situ PAR data collected during the CTD casts or estimated using the derived attenuation coefficients. Integrated, euphotic zone productivity was estimated by trapezoidal integrations of the 1-m estimates from the surface to the 1% isolume. Integrated daily productivity at all stations used the measured surface PAR data starting upon recovery of the CTD cast and continuing for 24 h. All integrated daily PAR data included dark periods at night.

A second method of estimating integrated productivity was used, based on surface temperature and chlorophyll distributions (Behrenfeld and Falkowski, 1997a, 1997b). Productivity was estimated from surface chl *a* concentration, daily irradiance (PAR), day length (DL), euphotic zone depth (the depth to which 1% of surface irradiance penetrates), and the optimum photosynthetic rate (P_{opt}^B) of phytoplankton (Eq. (3)):

$$PP_{eu} = 0.66125 \times P_{opt}^B \times \left[\frac{E_0}{E_0 + 4.1}\right] \times Z_{eu} \times Chl\ a \times DL \quad (3)$$

where PP_{eu} is the integrated daily euphotic zone productivity (mg C m^{-3} d^{-1}), P_{opt}^B is the optimum photosynthetic rate (mg C (mg Chl a)$^{-1}$ h^{-1}), E_0 is daily PAR at the seawater surface (mol photons m^{-2} d^{-1}), Z_{eu} is euphotic depth (m), Chl *a* is surface Chl *a* concentration (mg Chl *a* m^{-3}), and DL is the daily photoperiod (h). P_{opt}^B was estimated the temperature-dependent equation from Behrenfeld and Falkowski (1997b). The two models are different in that the first provides vertically resolved rates, while the second provides estimates based on surface chlorophyll.

Net seasonal production was estimated from nutrient deficits (Bates et al., 1998; Smith Jr. and Asper, 2000). Deep-water concentrations were taken from Bagøien et al. (2012), who compiled nutrient and mixed layer depths from coastal Norway and the Atlantic waters offshore. Winter mixed-layer depths in coastal waters averaged ca. 50 m, and in Atlantic waters >200 m. Winter (before chlorophyll levels increased above 0.25 mg m^{-3}) nitrate and silicic acid concentrations in coastal waters are 8 and 4 μM, respectively, and in Atlantic water 12 and 5 μM. Net seasonal removal was estimated from Eq. (4):

$$\Delta NO_3 = \int_{50}^{0} NO_3(winter) - \int_{50}^{0} NO_3(obs) \quad (4)$$

where ΔNO_3 is the seasonal nitrate removal (μmol m^{-2}), $NO_3(winter)$ is the integrated (from 0 to 50 m) winter mixed-layer nitrate concentration, and $NO_3(obs)$ is the measured integrated nitrate concentration at each station during the period of observations. The deficits were converted to carbon units using the Redfield ratio. Silicic acid reductions were also calculated from Eq. (4) to estimate diatomaceous production and converting the Si removal to nitrogen and carbon units using a Si/N molar ratio of 1 (Brzezinski, 1985). Growth and nutrient removal were assumed to start on March 1. Daily net community production rates were estimated from the nitrate removal divided by the number of days of growth. Similarly, diatom net community production was derived from silicic acid removal after converting to carbon units.

Estimates of seasonal production are one dimensional and involve several assumptions. One is that lateral advection has a minor impact. While we have no data to confirm the validity of this assumption, based on the presence of strong fronts within the study area, it is likely that errors introduced in this area are minor, especially when comparing coastal vs. open ocean stations. Advective changes in vertical mixing rates are likely minor relative to the changes due to biological processes. Such estimates have been conducted previously (e.g., Bates et al., 1998) and are an approximation of seasonal production.

2.7. Satellite chlorophyll a data

To place our observations within a broader seasonal progression of phytoplankton biomass in spring, satellite chlorophyll *a* data were taken from the NASA Ocean Color archive (https://oceancolor.gsfc.nasa.gov) to generate a regional climatology. A total of 128 remote sensing images from March to May in 2000–2019 using Level 2 data from the MODIS Terra and Aqua satellites and the VIIRS mission (4 km resolution) were processed to generate the climatology. Clouds, darkness, and angle between sunlight and satellite sensors limit ocean color sensor signals in high latitude systems; given the frequent cloudy conditions found in northern Norway during spring, only limited chlorophyll *a* data were available during March to May. We binned chlorophyll *a* data into 10-day intervals to generate the satellite climatology.

2.8. Data processing

Mixed layer depths (MLD) were determined from CTD, MVP and glider density profiles using the threshold method. MLD was defined as the depth at which seawater potential density changed by 0.03 kg m^{-3} relative to the potential density at 5 m. One complete oscillation of each instrument was averaged to give a profile for use in the models. Both MVP and glider data were interpolated to standard depths and locations before MLD calculation. Brunt-Väisälä frequencies (N^2) were calculated as a function of absolute salinity, conservative temperature, sea pressure and latitude, and were determined by using Gibbs-SeaWater toolbox (TEOS-10). Absolute salinity was calculated from practical salinity, sea pressure, longitude, latitude. Conservative temperature was calculated from absolute salinity, in-situ temperature and sea pressure. Practical salinity, sea pressure, in-situ temperature, longitude and latitude were accessed from CTD observations.

2.9. Statistical analysis

Linear regressions were performed using a least-square analysis, and the coefficient of determination (R^2) was applied to show the percentage of the variability attributable to the response. *P*-values were calculated using an F-test, with significance levels set a priori at 0.05. A two-sample *t*-test was performed to examine whether the differences that occurred between the two tested samples were significant. All statistical analyses were performed using MATLAB version R2020b.

3. Results

3.1. Hydrography

Sea surface temperatures (SST) ranged between 5.34 and 7.56 °C, and daily surface PAR ranged between 4.57 and 30.4 mol photons m^{-2} d^{-1}. Colder waters (<6.5 °C) were generally confined to the shelf, although they were also observed over the continental slope near the end of our cruise when the front delineating Norwegian Coast Current (NCC) and Norwegian Atlantic Slope Current (NwASC) broke down and

shelf-slope exchanges occurred (Dong et al., 2021). Surface salinities ranged between 33.5 and 34.8, with fresher waters (<34.6) being largely confined to the shelf (Figs. 2,3,4). Northern slope salinities ranged between 34.1 and 35.1, indicative the presence of both Norwegian Coastal Water (NCW) and North Atlantic Water (NAW). Mixed layer depths were generally between 9 and 50 m (Table 1, Table A2), being shallow within the southern shelf and northern shelf-break stations (13 ± 2.8 and 13 ± 6.3 m; Table 1). Brunt-Väisälä frequencies fluctuated in the upper 50 m (Table A2); higher N^2 values were found in the northern shelf break and slope region, with a mean value of 8.40 × 10^{-5} s^{-1}. The N^2 from the northern shelf stations and stations located in the NCW were greater than the N^2 from deep-water stations and those in the NAW, indicating that near-shore waters were more strongly stratified than the offshore waters.

Mixed layer nitrate and silicic acid concentrations increased from the shelf to deep waters. Mean mixed-layer nutrient concentrations in the southern shelf were lower than at northern shelf stations, and both phosphate and silicic acid concentrations were significantly lower than at the northern shelf stations as well ($p < 0.05$, Table 1, Table A2).

3.2. Phytoplankton distributions

The climatology derived from remotely sensed chlorophyll *a* data showed that phytoplankton blooms are usually initiated along the coast and move progressively offshore, and were separated by less than a few weeks (Fig. 5). Similarly, blooms also occurred earliest in the south and spread northward, reaching a maximum in mid-April. Substantial spatial variability in the timing of bloom appearance was noted, with a few offshore locations showing earlier growth and accumulation than the rest of offshore waters. Only one clear-sky image was available during the cruise (April 28; Fig. 6). It showed that waters on the continental shelf had lower chlorophyll levels than those of offshore waters, which exhibited broadly distributed concentrations >5 mg m^{-3}. Our maximum observed values (measured in offshore waters) were similar with those found in the climatology (ca. 5 mg m^{-3}; Figs. 2,3,4) and the April 26 image (Fig. 6).

Euphotic zone depths ranged between 19 and 50 m (Table A2) and were shallower in deep-water stations (27 ± 6.4 m) relative to shelf-break and inshore stations (Table 2). Surface chl *a* ranged between 0.27 and 5.68 mg m^{-3}, and surface POC, PON and BSi ranged between 0.72 and 8.95, 0.12–1.49 and 2.15–22.5 mmol m^{-3}, respectively (Table A3). Average mixed layer chl *a*, POC, PON and BSi levels all tended to increase along an inshore-offshore gradient, and BSi concentrations suggested that phytoplankton biomass was dominated by diatoms. Average mixed layer nitrate and silicic acid showed a similar pattern. This suggests that the spring bloom, especially that on the continental shelf, had largely occurred prior to our observations and that blooms developed in offshore waters during late April and early May, consistent with the satellite climatology and the single image available (Figs. 5, 6). BSi concentrations ranged between 1.34 and 22.5 μmol L^{-3}; C/N molar ratios in the surface water ranged between 3.31 and 8.17 and averaged 6.08 ± 1.54 for all euphotic zone samples. Surface POC/chl *a* ratios ranged between 10.9 and 77.5. Inshore waters had higher POC/chl *a* ratios than offshore waters (Table A3).

3.2.1. Temporal distributions

The highest chlorophyll concentrations were observed in offshore waters within transect T2 (April 25) and tended to decrease through time, consistent with the climatology. Such changes might be caused in part by the decrease in strength of the shelf break salinity front with time, which likely resulted from the disruption of the transport barrier in late spring by eddy activity (Dong et al., 2021). Surface chlorophyll

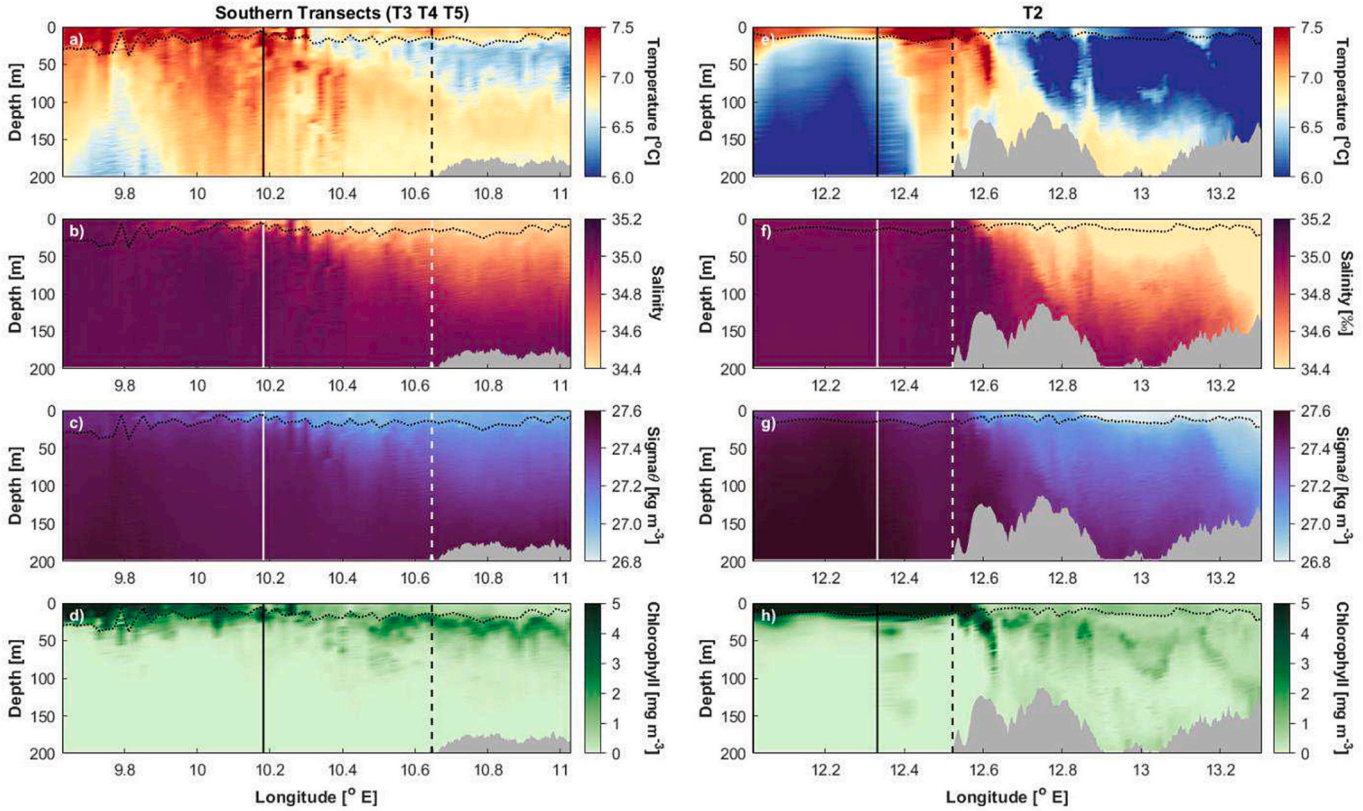

Fig. 2. Distribution of temperature, salinity, density (expressed as σ_θ) and chlorophyll in the upper 200 m within Transects 3–5 and Transect 2. Data from Transects 3–5 merged into a single mean distribution due to the closeness in time of sample collection. The dashed and solid lines represent the 200 and 1000 m locations. The dotted line represents the depth of the mixed layer.

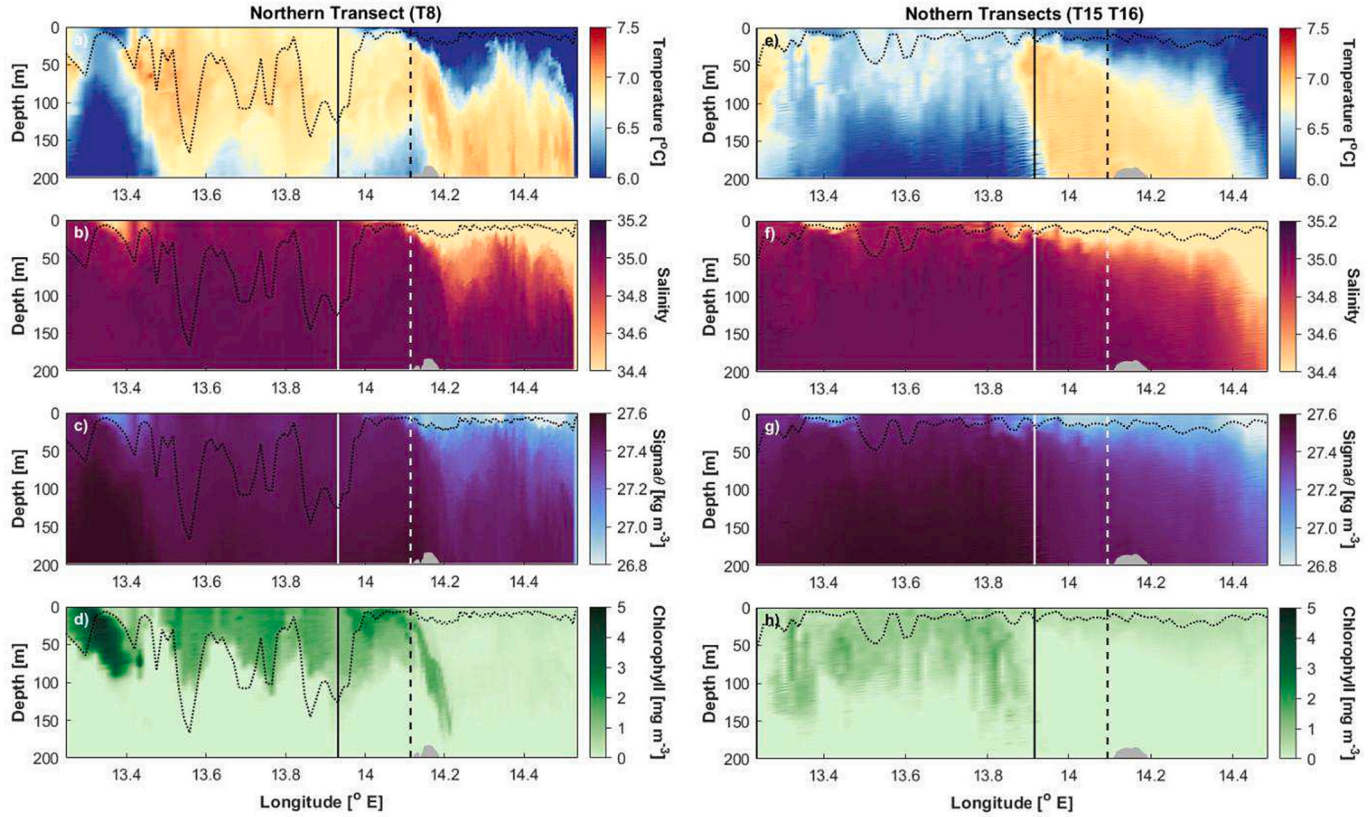

Fig. 3. Distribution of temperature, salinity, density (expressed as σ_θ) and chlorophyll in the upper 200 m within Transect 8 and Transect 15–16. Data from Transects 15 and 16 merged into a single mean distribution due to the closeness in time of sample collection. The dashed and solid lines represent the 200 and 1000 m locations. The dotted line represents the depth of the mixed layer.

concentrations also decreased through time and became concentrated at depth (usually below the base of the mixed layer). Integrated euphotic zone chlorophyll concentrations generally decreased with time, although the trend was most obvious at deep-water stations (Table A3). Glider fluorescence doubled offshore starting on April 28 (Fig. 4), and shelf fluorescence was low during both occupations.

3.2.2. Spatial distributions

Surface and integrated euphotic zone chlorophyll *a* concentrations ranged between 0.27 and 5.68 mg m^{-3} and 7.65 and 104 mg m^{-2}, respectively; stations located in the northern NAW showed significantly greater concentrations (both at the surface and in integrated values) than the NCW stations ($p < 0.001$, Table A3). Chlorophyll *a* concentrations observed by the MVP were higher in offshore waters than inshore on all transects regardless of the date of sampling (Figs. 2, 3). Fluorescence observed by the glider also showed the same trend (Fig. 4). Maximum Chl *a* concentrations occurred within mixed layer in offshore waters, but below the mixed layer in the inshore waters on transects T2, T3, T4, T5 and T8 (Figs. 2, 3). Compared with transect T8, both mixed layer depth and chl *a* concentrations were less than within transects T15 and T16 (sampled six days later; Fig. 4).

3.3. Primary productivity

Primary productivity was lowest on the continental shelf and increased in deeper waters, regardless of the method of estimation (Table 2). In general productivity estimated by the vertically resolved model was less than that determined from surface properties (Table 2). The two estimates were significantly correlated ($R^2 = 0.90$, $p < 0.001$), with the surface estimates being 29% greater on average than the vertically resolved model. Surface primary productivity ranged between 9 and 284 mg C m^{-3} d^{-1} (Table A3) and was significantly greater in the stations located in NAW ($p < 0.001$, Table A3). Primary productivity also was estimated along the MVP transects and ranged from 62 to 2350 mg C m^{-2} d^{-1} (Fig. 7). Productivity was greatest in deep water and was reduced on the shelf in all 7 transects. Seasonal production estimated from nutrient deficits was much less than.

that estimated from the bio-optical models (Table 3), which was not surprising given the vastly different time scales involved. It was broadly similar throughout the region, but slightly less on the northern shelf, where nutrients still remained in the surface layer and were fueling active new production. Estimates of diatomaceous production were from 41 to 63% of total net community production, confirming the important role of diatoms in the spring bloom.

3.4. Relationship between zooplankton and phytoplankton distributions

The highest *C. finmarchicus* abundance within the 1.0–2.0 mm ESD size fraction was ca. 20,000 individuals m^{-3} and occurred in the northern transects 15 and 16 (Fig. 8d). *C. finmarchicus* abundance in the earlier transects was about a half that found in T15 and T16, with maxima reaching ca. 10,000 individuals m^{-3} (Figs. 8a,b,c). *C. finmarchicus* abundance maxima were generally associated with low chlorophyll concentrations in all transects (Fig. A1), but at all southern transects some depths with high chlorophyll concentrations and elevated zooplankton abundance were noted.

4. Discussion

4.1. Spatial and temporal variability of Norwegian coastal waters

Phytoplankton off the northern Norwegian coast exhibited

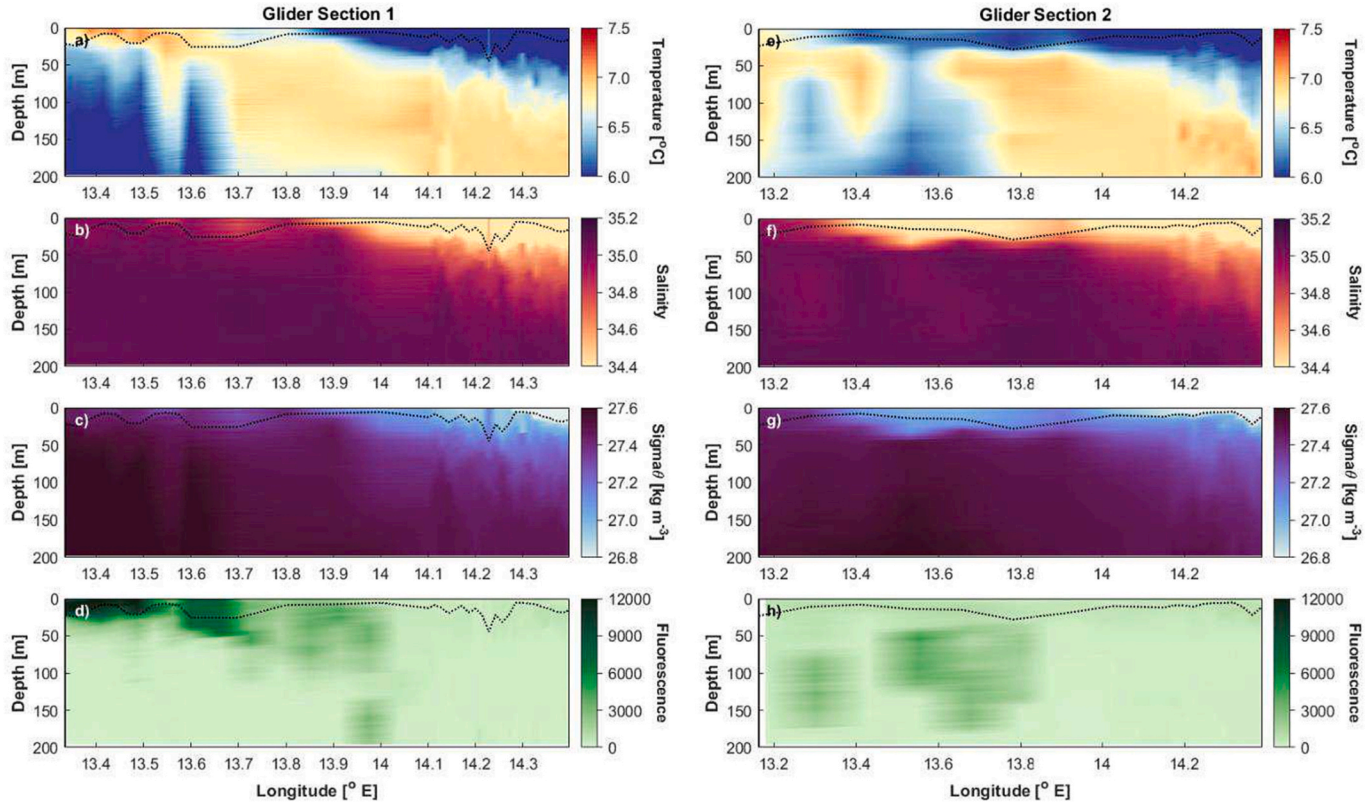

Fig. 4. Distribution of temperature, salinity, density (expressed as σ_θ) and fluorescence in the upper 200 m within Glider Transects 1 and 2. Fluorescence expressed in arbitrary units. The dotted line represents the depth of the mixed layer.

Table 1
Mean mixed layer (Z_{mix}) concentrations of nitrate (NO_3^-), phosphate (PO_4^{-3}), silicic acid ($Si(OH)_4$), and euphotic zone average concentrations of chlorophyll (chl *a*), particulate organic carbon (POC), particulate organic nitrogen (PON), and biogenic silica (BSi) (and their standard deviations) off the northern Norwegian coast. Stations grouped by location and depth (shelf <200 m; shelf break 200–400 m; slope 400–1000 m; deep water >1000 m). * = discrete samples lost; chl *a* estimated from CTD fluorescence data.

Location	Z_{mix} (m)	NO_3^- (μM)	PO_4^{-3} (μM)	$Si(OH)_4$ (μM)	Chl *a* (mg m^{-3})	POC (μmol L^{-1})	PON (μmol L^{-1})	BSi (μmol L^{-1})
Southern shelf (St. 7, 8)	13 ± 2.8	0.35 ± 0.05	0.09 ± 0.03	0.58 ± 0.01	0.67 ± 0.31*	1.84 ± 0.16	0.36 ± 0.09	3.55 ± 0.19
Northern shelf (St. 3, 4, 11, 14, 17–19, 23, 28)	22 ± 8.5	1.87 ± 1.11	0.24 ± 0.07	0.97 ± 0.23	0.59 ± 0.28*	1.29 ± 0.69	0.23 ± 0.14	3.89 ± 1.13
Northern shelf break (St. 9, 16)	13 ± 6.3	0.61 ± 0.56	0.51 ± 0.22	0.60 ± 0.14	0.45 ± 0.04	2.59 ± 2.03	0.49 ± 0.44	3.28 ± 0.18
Northern slope (St. 2, 6, 12, 15, 20, 22, 24, 27)	17 ± 4.2	1.68 ± 0.68	0.30 ± 0.23	1.35 ± 0.49	1.62 ± 1.57*	2.00 ± 1.49	0.31 ± 0.20	5.61 ± 3.95
Deep water (St. 1, 5, 10, 13, 21, 25, 26)	33 ± 16.0	3.04 ± 2.13	0.28 ± 0.10	1.54 ± 0.67	2.19 ± 1.35*	2.86 ± 2.01	0.58 ± 0.36	6.67 ± 3.53

substantial spatial variability that reflected the rapid growth and accumulation within the sub-polar spring bloom. Despite the relatively short sampling period, the use of multiple sampling modes allowed us to characterize the stage of the bloom over broad areas. The climatology clearly showed the temporal and spatial scales of variability (Fig. 5). Satellite-derived chlorophyll concentrations were low through March but increased substantially by mid-April to concentrations >5 mg m^{-3}, similar to the maxima found within our survey. These increases were largely confined to the continental shelf in waters that likely had increased stratification resulting from land-based inputs of fresher water. The high chlorophyll concentrations on the shelf were reduced rapidly (over ca. two weeks) but remained >2 mg m^{-3} over broad areas of the shelf. Some areas in deep waters also exhibited high chlorophyll concentrations in mid-April, and these may have resulted from the advective transport of phytoplankton when the density barrier at the shelf break was disrupted due to increased eddy activity during this period (Dong et al., 2021).

Waters on the continental slope and deeper areas supported the growth and accumulation of phytoplankton later than those on the shelf. This is clearly shown by the climatology, the single image obtained during our field observations, and the field measurements themselves. Concentrations of chlorophyll to the west of the shelf break were substantial (> 5 mg m^{-3}) and equal to those that occurred earlier on the continental shelf. Thus, any transfer of primary production through the food web would be similar in both regions and not simply confined to shallow waters, despite the differing phenology of the two areas.

The climatology does not address aspects of interannual variability, which is also substantial (Fig. 9). Such variability potentially can influence the coupling between phyto- and zooplankton and could have food-web implications. That is, some years the physical-biological coupling could be strong and facilitate an efficient transfer of organic matter to higher trophic levels, but in other years the reduced coupling could weaken such transfers. Understanding the magnitude of such variability and the strength of the biophysical coupling would contribute to the effective management of Norwegian fisheries.

Primary productivity in the region is substantial, but also shows the same variability as shown by chlorophyll distributions. This is not unexpected, as the estimates derived from the bio-optical model are

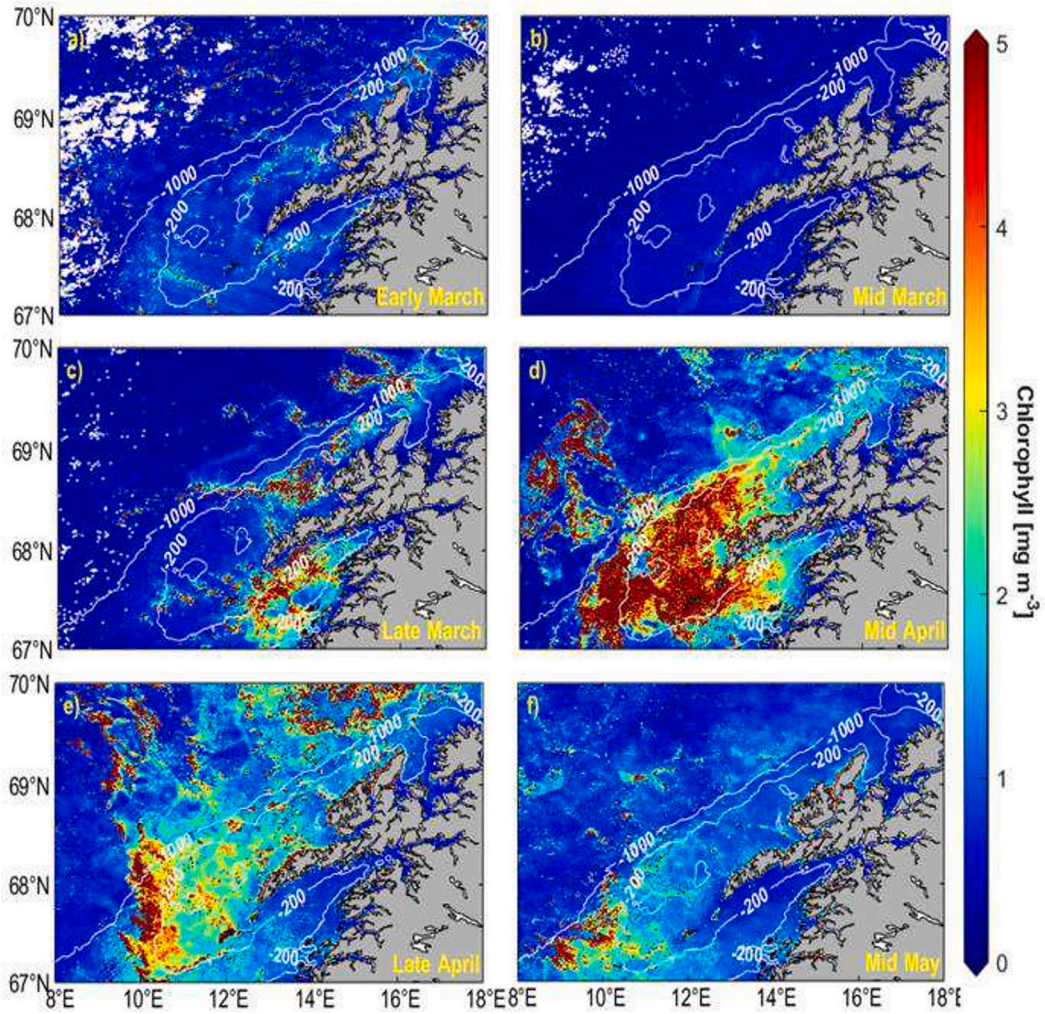

Fig. 5. Seasonal chlorophyll climatologies generated from satellite imagery. a) early March (March 1–10), b) mid-March (March 11–20), c) late March (March 21–31), d) mid-April (April 11–20), e) late April (April 21–30), and f) mid-May (May 11–20). Data were binned into 10-day intervals.

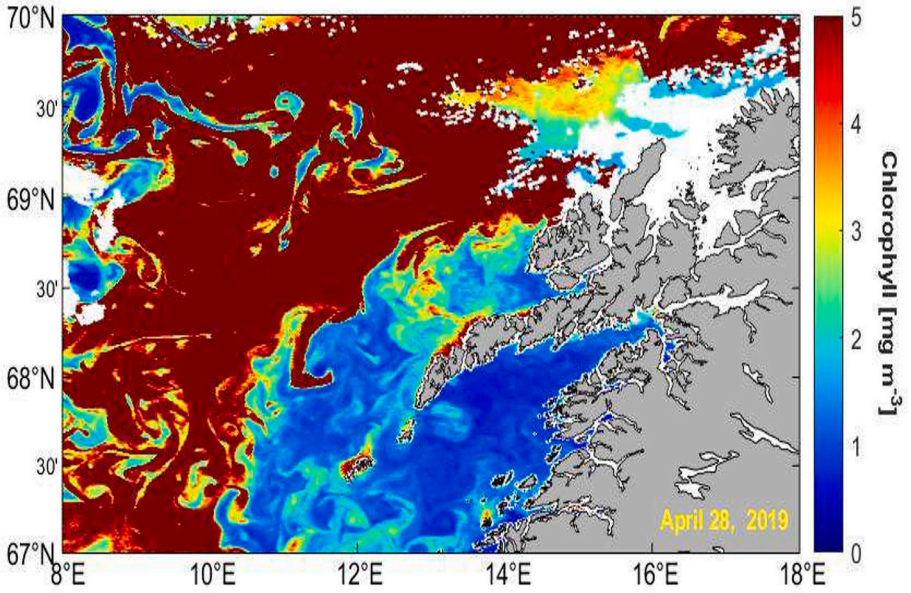

Fig. 6. MODIS image of chlorophyll concentrations in the study area on April 28, 2019.

Table 2
Mean euphotic zone depths (Z_{eu}, 1% isolume) and modeled primary productivity (and standard deviations) off the Norwegian coast. Stations grouped by location (south and north) and depth (shelf <200 m; shelf break 200–400 m; slope 400–1000 m; deep water >1000 m). PP1 is the euphotic zone integrated primary productivity based on the vertically resolved model (Eqs. (1) and (2)); PP2 is based on Eq. (3).

Location	Z_{eu} (m)	PP1 (mg C m^{-2} d^{-1})	PP2 (mg C m^{-2} d^{-1})
Southern shelf (St. 7, 8)	33 ± 2.8	217 ± 30	458 ± 18
Northern shelf (St. 3, 4, 11, 14, 17–19, 23, 28)	34 ± 9.0	216 ± 87	460 ± 167
Northern shelf break (St. 9, 16)	43 ± 7.8	196 ± 24	472 ± 73
Northern slope (St. 2, 6, 12, 15, 20, 22, 24, 27)	32 ± 7.3	513 ± 558	937 ± 778
Deep water (St. 1, 5, 10, 13, 21, 25, 26)	27 ± 6.4	660 ± 327	1357 ± 739

dependent on chlorophyll concentrations. Few productivity measurements have been reported from this area, which is surprising given the importance of quantifying the input of organic matter into *Calanus*-based food webs. The vertically resolved model provided estimates that were ca. 70% of those derived from the surface chlorophyll-derived method. Maximum productivity was >2 g C m^{-2} d^{-1}, consistent with estimates of productivity in the region (Wassmann and Aadnesen, 1984; Paasche, 1988) and of other sub-polar systems (Harrison et al., 2013; Richardson and Bendtsen, 2021). We believe the estimates derived from the vertically resolved model (PP1; Table 2) are more likely closer to the realized productivity due to the inclusion of the photoinhibition term, which is not included in surface chlorophyll-derived estimates (PP2; Table 2). Indeed, when that term is removed, no statistical difference between the two is noted. Estimates based on Eq. (4) also may not adequately resolve the influence of the deep chlorophyll maximum. Both are estimates of the amount of photosynthetic carbon entering the system and available for food-web processes. The strength of the density front impacted the magnitude of changes from shelf water to deep water, as productivity was much greater offshore during periods when a steep physical front was present (Figs. 7b,c), whereas it increased gradually in transects with a weakened physical front (Figs. 6a,d). Regardless of the

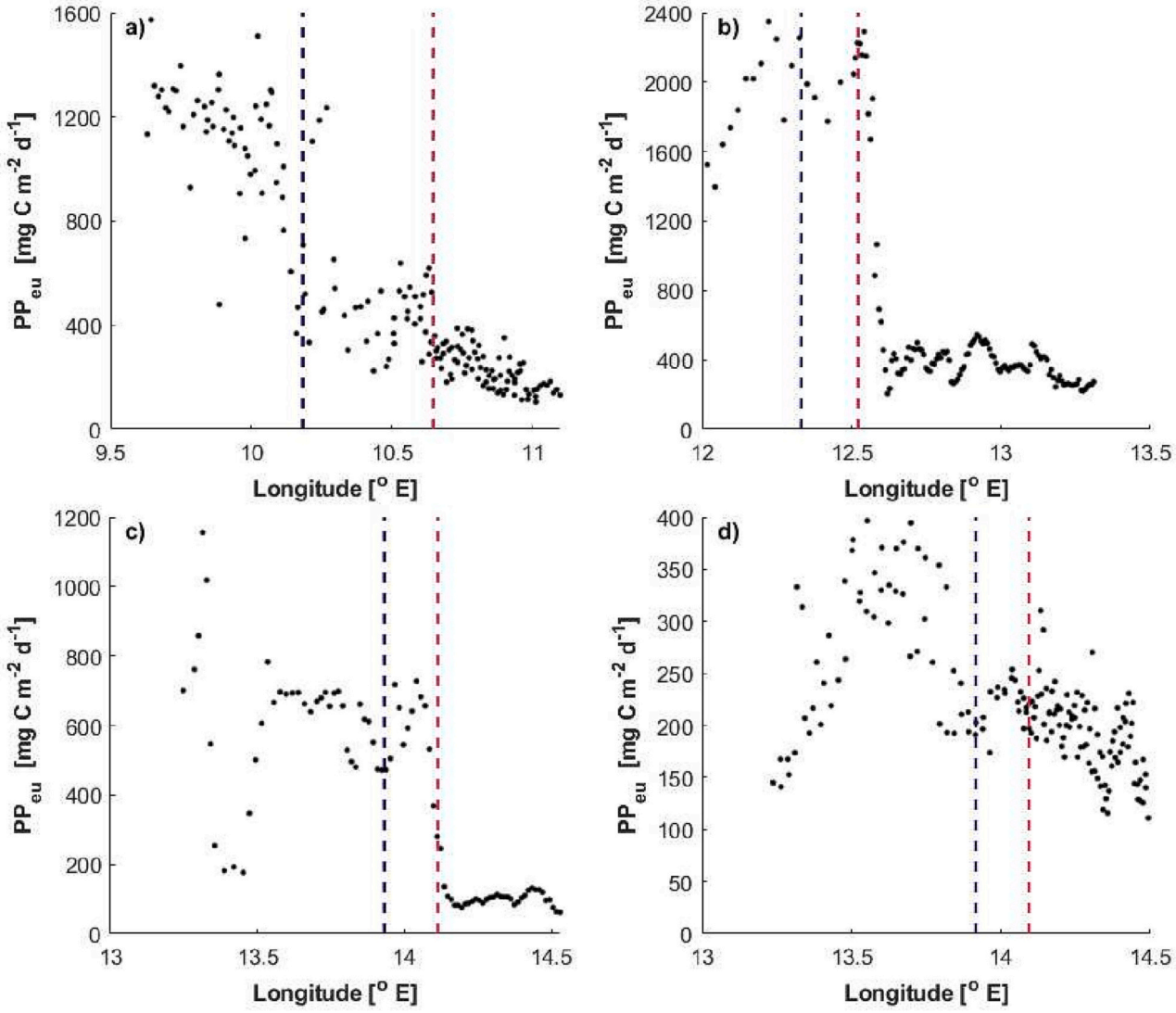

Fig. 7. Integrated primary productivity estimated from the moving vessel profiler from the vertically resolved model. a) transects T3, T4 and T5; b) transect T2; c) transect T8; d) transects T15 and T16. Red and blue dashed lines represent the location of 200 and 1000 m bottom depth. (For interpretation of the references to color in this figure legend, the reader is referred to the web version of this article.)

Table 3
Means and standard deviations of net seasonal drawdown of nitrate and silicic acid and the derived net community production (NCP) derived from nitrate and silicic acid removal (ΔNO_3 and $\Delta Si(OH)_4$) off the Norwegian coast as determined from seasonal nitrate and silicic acid deficits of the upper 50 m of the water column (Eq. (4)). NCP_{Si}/NCP_N is the percentage of NCP attributable to diatoms. Stations grouped by location (south and north) and depth (shelf <200 m; shelf break 200–400 m; slope 400–1000 m; deep water >1000 m).

Location	ΔNO_3 (μmol m^{-2})	$\Delta Si(OH)_4$ (μmol m^{-2})	NCP_N (mg C m^{-2} d^{-1})	NCP_{Si} (mg C m^{-2} d^{-1})	NCP_{Si}/NCP_N (%)
Southern shelf (St. 7, 8)	304 ± 80.9	157 ± 15.7	34.4 ± 7.91	20.5 ± 2.04	63
Northern shelf (St. 3, 4, 11, 14, 17–19, 23, 28)	212 ± 78.4	127 ± 21.8	21.7 ± 9.35	12.9 ± 3.07	60
Northern shelf break (St. 9, 16)	313 ± 32.3	153 ± 19.6	32.1 ± 4.69	15.6 ± 2.68	49
Northern slope (St. 2, 6, 12, 15, 20, 22, 24, 27)	167 ± 70.7	94.7 ± 31.5	21.7 ± 9.35	12.9 ± 3.07	57
Deep water (St. 1, 5, 10, 13, 21, 25, 26)	327 ± 73.2	133 ± 26.1	33.4 ± 8.98	13.6 ± 3.16	41

uncertainties, these rates demonstrate the productive nature of the Norwegian shelf-slope region during spring.

4.2. Controls on the vertical distribution of chlorophyll

Vertical chlorophyll maxima were often found associated with hydrographic discontinuities. Deep chlorophyll maxima (DCM) can have multiple mechanisms of formation (Cullen, 2015), but the mechanism generating DCM in MVP Transect 2 appeared to be the physical advection of phytoplankton to depth (Fig. 2). At 12.6°E a strong front occurred as evidenced by the temperature distribution, and resulted in a flow of warm, offshore water to depth. This water contained larger concentrations of chlorophyll, which generated a DCM at that location. Similarly, a mesoscale feature at ca. 12.85°E upwelled warm water with elevated chlorophyll towards the surface. Inshore of that feature, chlorophyll maxima occurred at sub-euphotic depths and were associated with temperature and salinity discontinuities (Fig. 2). However, not all DCM were associated with physical features (e.g., Transect 3–5, Fig. 2; Glider Transects, Fig. 4). At these locations chlorophyll may have increased at depth due to acclimation to low irradiance levels, accumulation from passive sinking on density discontinuities (whose sinking rates may have been enhanced by nutrient limitation) and in situ growth.

4.3. Relationship between chlorophyll and zooplankton

The spatial and temporal variability of the region was also expressed in the relationship between chlorophyll concentrations and *Calanus finmarchicus* abundance. Within a spring bloom, zooplankton biomass lags phytoplankton growth and accumulation due to the effects of temperature on zooplankton development (Cushing, 1995; Søreide et al., 2010; Daase et al., 2013). Hence, at any time phytoplankton and zooplankton can be negatively (phytoplankton increasing when zooplankton biomass is low, or when zooplankton are high and phytoplankton levels have been reduced) or positively (when both are increasing) correlated. These relationships appear to be expressed in our data (Fig. 8, FigureA1). In the earliest occupation (Transect 2, April 29), chlorophyll on the shelf was relatively low, and zooplankton abundance was relatively uniform over the shelf, and zooplankton maxima occurred in low chlorophyll waters (Fig. 8b, A1). This may indicate a period when

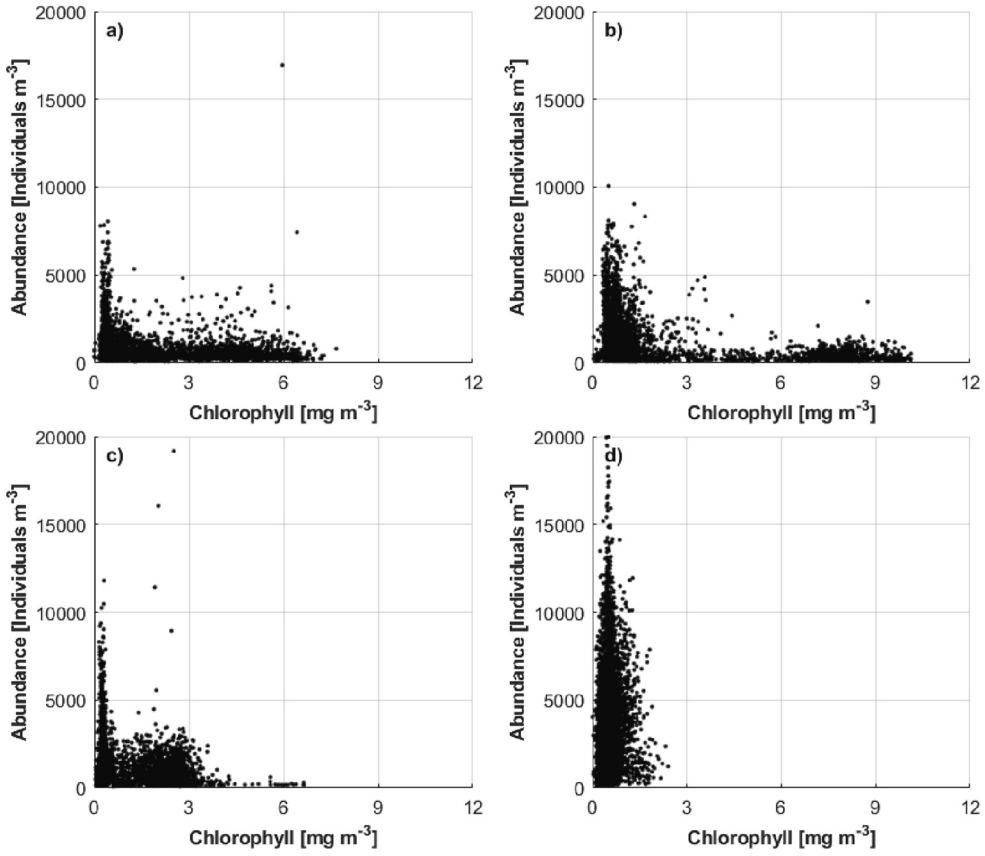

Fig. 8. Relationship between copepod abundance and chlorophyll. Copepod abundance was estimated from particle abundance between 1 and 2 mm ESD in the upper 30 m. a) transects T3, T4 and T5; b) transect T2; c) transect T8; d) transects T15 and T16.

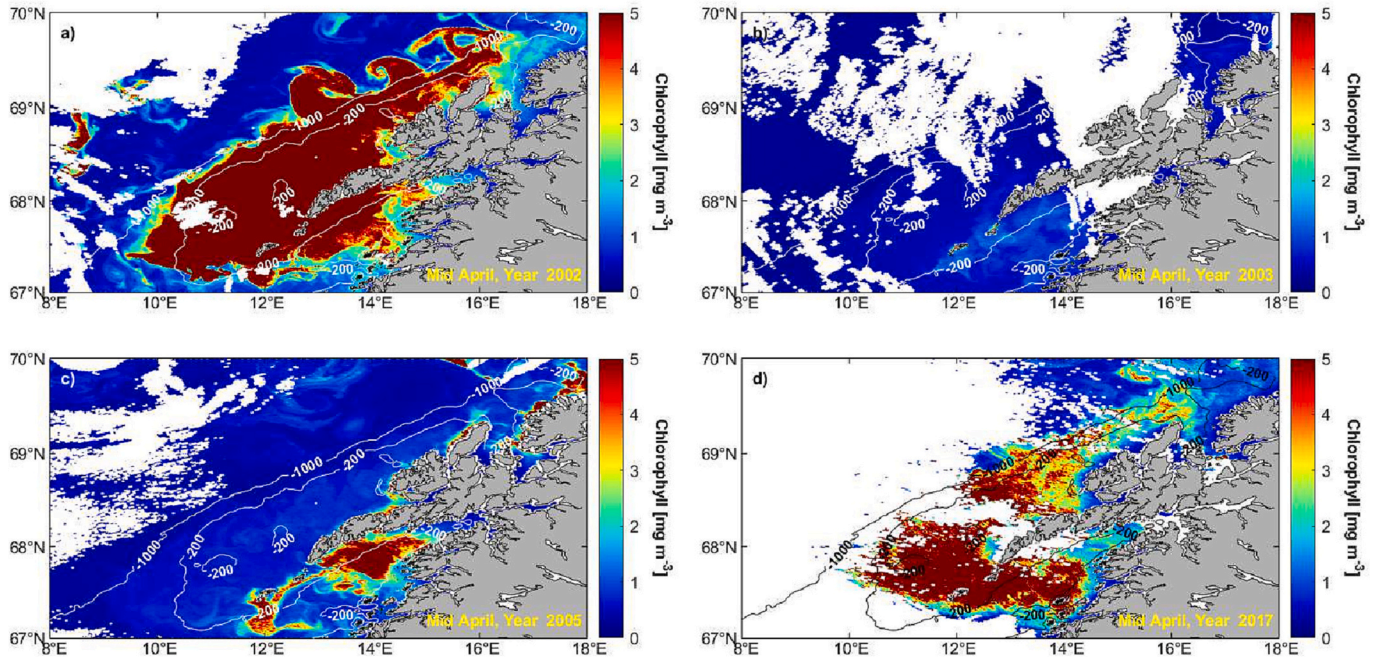

Fig. 9. Examples of interannual variability in chlorophyll concentrations off the Lofoton coast. All images are from approximately the same date in mid-April. a) 2002, b) 2003, c) 2005, and d) 2017.

phytoplankton biomass in the upper 30 m had been reduced either by sinking to depth or grazing. During April 30 (Transects 3–5), there were a number of depths where the low chlorophyll-elevated zooplankton abundance relationship was observed, suggesting a period where zooplankton biomass had increased and phytoplankton chlorophyll had decreased, possibly as a result of grazing (Fig. 8a). Chlorophyll maxima were again located below the mixed layer, and chlorophyll maxima were observed around and below the depth of euphotic layer at Stations 7 and 8. Six days later (Transect 8, May 5; Fig. 8c), the pattern was like that found on April 30 – relatively enhanced zooplankton abundance associated with lower chlorophyll on the shelf (Transect 8, Fig. A1). Within Transects 15–16 (May 10–11), the relationship was notably different, in that there were no chlorophyll concentrations >2.4 mg m^{-3} and zooplankton biomass was elevated over much of the transect (Fig. 8d), both chlorophyll concentrations and copepod abundance were uniform (Fig. A1). We suggest that growth of both zooplankton and phytoplankton were more tightly coupled at this time and location, especially since much of the frontal structure had dissipated by this time (Dong et al., 2021). In view of the spatio-temporal variability that occurs throughout the region, understanding the coupling between phytoplankton and zooplankton is challenging.

Because *Calanus finmarchicus* reaches such massive accumulations to allow it to be observed by satellites (Basedow et al., 2019; Dong et al., 2021), we expected that the copepod populations could exert a substantial influence on phytoplankton biomass. Irigoien et al. (1998) sampled from March – June in the deep waters off Norway and estimated that *C. finmarchicus* used ca. 15% of the chlorophyll per day during the bloom period (chlorophyll concentrations ≥3 mg Chl m^{-3}) and 5% per day post-bloom. Using their experimentally determined average ingestion rate (7.59 ng C individual^{-1} d^{-1}) and their mean C/chl ratio of 62 (Irigoien et al., 1998) with the mean abundances of *C. finmarchicus* we found in the upper 30 m along all MVP transects, we estimate that *Calanus* grazing removed from 1.36 to 14.6 mg chl m^{-3} d^{-1} (Table 4). Removal in Transects 2–8 (all completed before May 5) was <25%, while in the two northern transects (15 and 16, sampled on May 10–11) daily removal was between 52 and 69%. Removal largely varies with *Calanus* abundance, which was higher in the north. These estimates have substantial uncertainty, given the spatial variability in productivity and

Table 4
Estimates of potential chlorophyll removal (Chl_{rem}) by *Calanus finmarchicus* grazing on each MVP transect. Ingestion rate used was 7.59 ng C ind^{-1} d^{-1} (Irigoien et al., 1998) and were converted into chlorophyll units using their C/chl ratio of 62. Chlorophyll concentrations (Chl) and *C. finmarchicus* abundances are the means in the upper 30 m determined from fluorescence and the LOPC. Chlorophyll production (Chl_{prod}) rates were calculated from the productivity of each descent of the MVP estimated from the vertically resolved model and converted into chlorophyll units using a C/chl ratio of 40. Daily removal is the percentage of the chlorophyll removed relative to the total chlorophyll pool (initial plus production). Production/Removal is the ratio of Chl_{prod} to Chl_{rem}; values >1 indicate that chlorophyll was increasing.

Transect	Chl (mg m^{-3})	*Calanus* Abundance (ind m^{-3})	Chl_{prod} (mg chl m^{-2} d^{-1})	Chl_{rem} (mg chl m^{-2} d^{-1})	Daily Removal (%)	Production/ Removal
3	1.89	678	14.39	2.49	7.43	15.0
4	1.91	369	14.63	1.36	3.37	26.1
5	2.40	515	12.64	1.89	3.61	10.5
2	2.09	994	16.9	3.65	11.6	15.6
8	1.17	1034	7.81	3.80	24.6	11.5
15	0.58	3986	5.66	14.6	69.2	0.84
16	0.53	2777	5.54	10.2	52.2	1.55

in the carbon/chlorophyll ratios used to convert our production rates into chlorophyll units. However, we further estimated the average percentage removal within each transect, and their potential changes in time (Table 4). Caution needs to be used in extrapolating them to broader regions, given the variability we observed without our study region. To better understand the impact of *Calanus* grazing under conditions of extreme biomass accumulations, estimates of ingestion rates, phytoplankton growth and biomass, and copepod abundance need to be completed at the same time and location.

The variability of estimated *Calanus* removal of chlorophyll within a single transect was also substantial. For example, within Transect 8 the daily removal ranged from 0.02 to 262%, with similar ranges at other transects (data not shown). As removal is largely controlled by *Calanus* abundance, this suggests that other factors may be influencing the sub-

mesoscale distributions of the copepod, such as vertical migration, movement in response to predation, and responses to other environmental parameters. The sub-mesoscale distributions of copepods likely has a strong influence on the trophic dynamics of the Norwegian shelf-slope region and deserve closer attention using modern assessments of biomass. In the southern transects (T2, T3 and T4) copepod abundance was greater on the shelf and correlated with low chlorophyll concentrations and a presumed high daily removal rate. In the Northern transects (T8, T15 and T16), before the density front had dissipated, deep waters had low copepod abundances, and higher copepod abundances were related with low chlorophyll concentrations. After the disruption of density front, copepod abundance increased and was elevated from the shelf to deep water region, and low chlorophyll concentrations and presumed large daily removal rates were observed along these transects (T15, T16).

Another estimate of the impact of zooplankton on phytoplankton distributions can be derived by combining the productivity rates with the particulate matter distributions to calculate the daily increase in POC (and chlorophyll) and comparing those estimates with the chlorophyll loss rates estimated by Irigoien et al. (1998). By estimating phytoplankton growth rates from the ratio of productivity and POC concentrations, and assuming exponential growth over one day, the increase in POC can be approximated (Table A4). The mean daily percentage increase in POC is >166%, almost equal to a doubling per day [consistent with the high primary productivity rates]. If a similar calculation is made using chlorophyll data (by converting the carbon production rates to chlorophyll production rates using a C:chl ratio of 40; Riemann et al., 1989), the mean percentage increase is 59%, less than that derived using carbon values (Table A4), due to the low C:chl ratios we occasionally observed.

The correlations between phytoplankton and *Calanus* biomass suggest that copepod grazing was having a strong impact on phytoplankton distributions, while combining rate measurements with observed phytoplankton biomass and growth suggests that such impacts were not uniformly distributed in space and time, and at times was minor. Further observations coupled with direct measurements of grazing are required to determine the relative magnitude of chlorophyll removal by micro- and mesozooplankton and the influence of physical processes in northern Norwegian waters to fully understand the role of grazing on phytoplankton distributions.

5. Conclusions

We characterized the northern Norwegian continental shelf/coast region with regard to phytoplankton distributions and its relationship to the dominant grazer, *Calanus finmarchicus*. The region is characterized by a spring bloom that first occurs on the shallow waters of the continental shelf, likely due to increased stratification by fresh-water inputs from land and proceeds northward and offshore over times scales of a few weeks. Substantial spatial and temporal variability occurs on all scales, which can potentially have important impacts on regional food webs. The coupling of phytoplankton and zooplankton also varies spatially. Primary productivity is substantial and follows patterns like those of chlorophyll, and diatoms contributed the majority of net community production. The biomass of *Calanus finmarchicus*, the dominant grazer in the system, was generally negatively correlated with chlorophyll, and we estimated that copepod populations potentially removed from 3 to 69% of the chlorophyll per day. Chlorophyll maxima observed occurred below mixed layer and euphotic zone, and these maxima appear to be related to both physical processes, copepod grazing and passive sinking.

Acknowledgments, samples, and data

This research was supported by grants from the National Science Foundation of China (Grant 41861134040) and the Norwegian Research Council (Grant 287043). We are very grateful to Ms. Yiwu Zhu, who assisted with the analysis of the optical plankton counter data, and thank the officers and crew of the *R.V. Helmar Hanson* for their assistance, as well as our Stressor colleagues for their help at sea.

Declaration of Competing Interest

The authors declare that they have no competing financial interests or personal relationships that could have influenced the work reported in this paper.

Data availability

The data sets are open access. Nutrient and particulate matter concentration data: https://doi.org/10.18710/ZVIJWA; moving vessel data (including the LOPC data): https://doi.org/10.18710/DXA0F3; meteorological data from the ship's instruments (water temperature, wind, air temperature, atmospheric pressure, humidity, PAR): https://doi.org/10.18710/AWV7EM. A full cruise report is available at https://doi.org/10.18710/KVPUTW. The ocean color data, including VIIRS and MODIS, were provided by the Ocean Biology Processing Group (https://oceancolor.gsfc.nasa.gov).

Appendix A. Supplementary data

Supplementary data to this article can be found online at https://doi.org/10.1016/j.jmarsys.2023.103891.

References

Bagøien, E., Melle, W., Kaartvedt, S., 2012. Seasonal development of mixed layer depths, nutrients, chlorophyll and *Calanus finmarchicus* in the Norwegian Sea – a basin-scale habitat comparison. Prog. Oceanogr. 103, 58–79. https://doi.org/10.1016/j.pocean.2012.04.014.

Basedow, S.L., Edvardsen, A., Tande, K.S., 2008. Vertical segregation of *Calanus finmarchicus* copepodites during the spring bloom. J. Mar. Syst. 70, 21–32. https://doi.org/10.1016/j.jmarsys.2007.02.023.

Basedow, S.L., McKee, D., Lefering, I., Gislason, A., Daase, M., Trudnowska, E., et al., 2019. Remote sensing of zooplankton swarms. Scien. Rep. 9, 686. https://doi.org/10.1038/s41598-018-37129-x.

Basedow, S.L., Tande, K.S., Norrbin, M.F., Kristiansen, S.A., 2013. Capturing quantitative zooplankton information in the sea: performance test of laser optical plankton counter and video plankton recorder in a *Calanus finmarchicus* dominated summer situation. Prog. Oceanogr. 108, 72–80. https://doi.org/10.1016/j.pocean.2012.10.005.

Bates, N.R., Hansell, D.S., Carlson, C.A., Gordon, L.I., 1998. Distribution of CO_2 species, estimates of net community production and air–sea CO_2 exchanges in the Ross Sea polynya. J. Geophys. Res. 103, 2883–2896.

Behrenfeld, M.J., Falkowski, P.G., 1997a. Photosynthetic rates derived from satellite-based chlorophyll concentration. Limnol. Oceanogr. 42, 1–20.

Behrenfeld, M.J., Falkowski, P.G., 1997b. A consumer's guide to phytoplankton primary productivity models. Limnol. Oceanogr. 42, 1479–1491.

Bouman, H.A., Platt, T., Doblin, M., Figueiras, F.G., Gudmundsson, K., Gudfinnsoson, H. G., et al., 2018. Photosynthesis-irradiance parameters of marine phytoplankton: synthesis of a global data set. Earth Syst. Sci. Data 10, 251–266. https://doi.org/10.5194/essd-10-251-2018.

Brzezinski, M.A., 1985. The Si:C:N ratio of marine diatoms: interspecific variability and the effect of some environmental variables. J. Phycol. 21, 347–357.

Brzezinski, M.A., Nelson, D.M., 1989. Seasonal changes in the silicon cycle within a Gulf Stream warm-core ring. Deep-Sea Res. 36, 1009–1030.

Cullen, J.J., 2015. Subsurface chlorophyll maximum layers: enduring enigma or mystery solved? Annu. Rev. Mar. Sci. 7, 207–239. https://doi.org/10.1146/annurev-marine-010213-135111.

Cushing, D., 1995. Population Production and Regulation in the Sea: A Fisheries Perspective. Cambridge Univ. Press, Cambridge, UK.

Daase, M., Falk-Petersen, S., Varpe, Ø., Darnis, G., Søreide, J.E., et al., 2013. Timing of reproductive events in the marine copepod *Calanus glacialis*: a pan-Arctic perspective. Can. J. Fish. Aquat. Sci. 70, 871–884.

Dong, H., Zhou, M., Hu, Z., Zhang, Zhong, Y., Basedow, S.L., Smith Jr., W.O., 2021. Transport barriers and the retention of *Calanus finmarchicus* on the Lofoten shelf in early spring. J. Geophys. Res. 126, e2021JC017408 https://doi.org/10.1029/2021JC017408.

Eppley, R.W., 1982. The PRPOOS program: A study of plankton rate processes in oligotrophic oceans. EOS. Trans. Am. Geophys. Union 163, 522. https://doi.org/10.1029/EO063i022p00522-01.

Friedrichs, M.A.M., Carr, M.-E., Barber, R.T., Scardi, M., Antoine, D., Armstrong, R.A., et al., 2009. Assessing the uncrtainties of model estimates of primary productivity in the tropic Pacific Ocean. J. Mar. Syst. 76, 113–133.

Gaardsted, F., Tande, K.S., Basedow, S.L., 2010. Measuring copepod abundance in deep-water winter habitats in the NE Norwegian Sea: intercomparison of results from laser optical plankton counter and multinet. Fish. Oceanogr. 19, 480–492. https://doi.org/10.1111/j.1365-2419.2010.00558.x.

Gardner, W.D., Richardson, M.J., Smith Jr., W.O., 2000. Seasonal patterns of water column particulate organic carbon and fluxes in the Ross Sea, Antarctica. Deep-Sea Res. II 47, 3423–3449.

Harrison, W.G., Børsheim, K.Y., Li, W.K., Maillet, G.L., Pepin, P., Sakshaug, E., et al., 2013. Phytoplankton production and growth regulation in the Subarctic North Atlantic: A comparative study of the Labrador Sea-Labrador/Newfoundland shelves and Barents/Norwegian/Greenland seas and shelves. Prog. Oceanogr. 114, 26–45. https://doi.org/10.1016/j.pocean.2013.05.003.

Herman, A., Beanlands, B., Phillips, E., 2004. The next generation of optical plankton counter: the laser-OPC. J. Plankton Res. 26, 1135–1145.

Irigoien, X., Head, R., Klenke, U., Meyer-Harms, B., Harbour, D., Niehoff, B., Harris, R., 1998. A high frequency time series at weathership M, Norwegian Sea, during the 1997 spring bloom: feeding of adult female Calanus finmarchicus. Mar. Ecol. Prog. Ser. 172, 127–137.

Kaufman, D.E., Friedrichs, M.A.M., Smith Jr., W.O., Queste, B.Y., Heywood, K.J., 2014. Biogeochemical variability in the southern Ross Sea as observed by a glider deployment. Deep-Sea Res. I 92, 93–106.

Lee, Z., Marra, J., Perry, M.J., Kahru, M., 2015. Estimating oceanic primary productivity for ocean color remote sensing: a stragic assessment. J. Mar. Syst. 149, 50–59.

Ma, J., Smith Jr., W.O., 2022. Primary productivity in the mid-Atlantic bight: is the shelf break a location of enhanced productivity? Front. Mar. Sci. 9, 824303 https://doi.org/10.3389/fmars.2022.824303.

Mahadevan, A., D'Asaro, E., Lee, C., Perry, M.J., 2012. Eddy-driven stratification initiates North Atlantic spring phytoplankton blooms. Science 337, 54–58.

Marra, J., 2009. Net and gross productivity: weighing in with ^{14}C. Aquat. Microb. Ecol. 56, 123–131.

Marra, J.F., Barber, R.T., Barber, E., Bidigare, R.R., Chamberlin, W.S., Goericke, R., et al., 2021. A database of ocean primary productivity from the ^{14}C method. Limnol. Oceanogr. Lett. 6, 107–111. https://doi.org/10.1002/lol2.10175.

Morel, A., 1974. Optical properties of pure water and pure seawater. In: Jerlov, N.G., Steemann Nielsen, E. (Eds.), Optical Aspects of Oceanography. Academic, San Diego, CA, pp. 1–24.

Morel, A., 1998. Optical modeling of the upper ocean in relation to its biogenous matter content (case I waters). J. Geophys. Res. 93, 10,749–10,768.

Mork, M., Swallow, J.C., Currie, R.I., Gill, A.E., Simpson, J.H., 1981. Circulation phenomena and frontal dynamics of the Norwegian coastal current. Philos. Trans. R. Soc. Lond. A 302, 635–647. https://doi.org/10.1098/rsta.1981.0188.

Paasche, E., 1988. Pelagic primary production in nearshore waters. In: Nitrogen Cycling in Coastal Marine Environments. John Willey & Sons, New York, pp. 33–57.

Pedersen, O., Zhou, M., Tande, K., Edvardsen, A., 2005. Eddy formation on the coast of North Norway–evidenced by synoptic sampling. ICES J. Mar. Sci. 62, 615–628.

Platt, T., Jassby, A.D., 1976. The relationship between photosynthesis and light for natural assemblages of coastal marine phytoplankton. J. Phycol. 12, 421–430.

Richardson, K., Bendtsen, J., 2021. Distinct seasonal primary production patterns in the sub-polar gyre and surrounding seas. Front. Mar. Sci. 8, 785685 https://doi.org/10.3389/fmars.2021.785685.

Riemann, B., Simonsen, P., Stensgaard, L., 1989. The carbon and chlorophyll content of phytoplankton from various nutrient regimes. J. Plankton Res. 11, 1037–1045. https://doi.org/10.1093/plankt/11.5.1037.

Ryan-Keogh, T.R., Smith Jr., W.O., 2021. Temporal patterns of iron limitation in the Ross Sea as determined from chlorophyll fluorescence. J. Mar. Syst. 215, 103500 https://doi.org/10.1016/j.jmarsys.2020.103500.

Sætre, R., 1999. Features of the central Norwegian shelf circulation. Cont. Shelf Res. 19, 1809–1831. https://doi.org/10.1016/S0278-4343(99)00041-2.

Skagseth, Ø., Drinkwater, K.F., Terrile, E., 2011. Wind- and buoyancy-induced transport of the Norwegian coastal current in the Barents Sea. J. Geophys. Res. 116 (C8) https://doi.org/10.1029/2011JC006996.

Smith Jr., W.O., Asper, V., 2000. A balanced nitrogen budget of the surface layer of the southern Ross Sea, Antarctica. Geophys. Res. Lett. 27, 2721–2724.

Smith Jr., W.O., Zhang, W.G., Hirzel, A., Stanley, R.H.R., Meyer, M.G., Sosik, H.M., et al., 2021. A regional, early spring bloom of *Phaeocystis pouchetii* on the New England continental shelf. J. Geophys. Res. 126, e2020JC016856 https://doi.org/10.1029/2020JC016856.

Søreide, J.E., Leu, E.V., Berge, J., Graeve, M., Falk-Petersen, S., 2010. Timing of blooms, algal food quality and *Calanus glacialis* reproduction and growth in a changing Arctic. Glob. Chang. Biol. 16, 3154–3163.

Steemann Nielsen, E., 1952. The use of radioactive carbon (C14) for measuring organic production in the sea. J. Conseil Int. Explor. Mer. 18, 117–140. https://doi.org/10.1093/icesjms/18. 2.117.

Wassmann, P., Aadnesen, A., 1984. Hydrography, nutrients, suspended organic matter, and primary production in a shallow fjord system on the west coast of Norway. Sarsia 69, 139–153.